Experimental and Modeling Study of Protein Adsorption in Expanded Bed

Ping Li, Guohua Xiu, and Alirio E. Rodrigues
Laboratory of Separation and Reaction Engineering, Dept. of Chemical Engineering, Faculty of Engineering, University of Porto, Rua Dr. Roberto Frias, s/n 4200-465 Porto, Portugal

DOI 10.1002/aic.10536
Published online July 19, 2005 in Wiley InterScience (www.interscience.wiley.com).

Streamline DEAE is the first-generation adsorbent developed for expanded bed adsorption (low-density base matrix with wide particle size distribution and ligand sensitive to ionic strength and salt concentration), and Streamline direct CST I is the second-generation adsorbent (high-density base matrix with narrow particle size distribution and ligand not sensitive to ionic strength and salt concentration). In this paper, experiments were carried out for bovine serum albumin (BSA) protein adsorption in expanded beds, where a Streamline 50 column was packed either with Streamline DEAE or with Streamline direct CST I. The hydrodynamics, BSA dynamic binding capacity, and BSA recovery in the whole expanded bed adsorption process were compared for both adsorbents. A mathematical model, in which intraparticle diffusion, film mass transfer, liquid axial dispersion, solid axial dispersion, particle size axial distribution, and bed voidage axial variation were taken into account, was developed to predict the breakthrough curves in expanded bed adsorption. BSA breakthrough curves in expanded bed adsorption were measured for both Streamline DEAE and Streamline CST I, and compared with the predictions from this mathematical model. The effects of intraparticle diffusion, film mass transfer, liquid and solid axial dispersion, particle size axial distribution, and bed voidage axial variation on the breakthrough curves were evaluated for expanded bed adsorption with both adsorbents. © 2005 American Institute of Chemical Engineers *AIChE J,* 51: 2965–2977, 2005

Keywords: expanded bed adsorption, protein adsorption kinetics, modeling, breakthrough curves, residence time distributions

Introduction

Expanded bed adsorption is a single operation in which desired proteins are purified from particulate-containing feedstocks without the need for separate clarification, concentration, and initial purification. This technology has been widely applied to capture proteins directly from crude feedstocks, such as *E. coli* homogenate, yeast, fermentation, mammalian cell culture, milk, animal tissue extracts, and other unclarified feedstocks, and various applications have been reported from lab-scale to pilot-plant and large-scale production.[1–9]

With specially designed adsorbents and columns, the adsorption behavior in expanded beds is comparable to that in fixed beds.[1] Streamline DEAE and Streamline SP are typical first-generation adsorbents, developed for expanded bed adsorption. The modified Sepharose matrices allow capture of biomolecules directly from unclarified feedstocks; the adsorbents have high binding capacities and product yields, attributed to stable

Correspondence concerning this article should be addressed to A. E. Rodrigues at arodrig@fe.up.pt.

expanded beds, and long life as the result of high chemical and mechanical stability. Many theoretical and experimental researches were reported in the literature[10-17] with respect to the hydrodynamics and protein adsorption kinetics in expanded beds packed with the first-generation adsorbents. Streamline direct CST I, a second-generation adsorbent recently developed for use in expanded bed adsorption, has two special features compared with the first-generation adsorbents: a high-density base matrix and a salt-tolerant ligand. The high-density matrix means minimizing dilution arising from biomass or viscosity and reducing dilution buffer consumption; the ligand's lack of sensitivity to ionic strength means there is no need for dilution of feedstock because of high ionic strength. However, hydrodynamics and protein adsorption kinetics in expanded beds packed with the second-generation adsorbent have not been investigated in detail.

In this article, experiments were carried out for protein [bovine serum albumin (BSA)] adsorption in expanded beds, where a Streamline 50 column was packed with 300 mL Streamline DEAE and with 300 mL Streamline direct CST I, respectively. The experimental results are compared for both adsorbents to give a comprehensive evaluation of the hydrodynamics, BSA dynamic binding capacity, and BSA recovery in the whole expanded bed adsorption process.

The hydrodynamics and adsorption kinetics in expanded beds are more complex than that in fixed beds. The liquid axial dispersion in expanded beds is more significant than that in fixed beds; because of the fluidized nature of the expanded bed, adsorbent particle axial dispersion occurs. Moreover, there are variations of particle size axial distribution and bed voidage axial in expanded beds for the specially designed adsorbents with wide particle size distribution.[11,15,16,18] Models available for fixed beds may be not adequate to describe the hydrodynamic and adsorption behavior in expanded beds.

Wright et al.[14] developed a mathematical model to predict the breakthrough curve for protein adsorption in a fluidized bed, where intraparticle diffusion resistance, film mass transfer resistance, liquid axial dispersion, and adsorbent particle axial dispersion were taken into account. Later, Tong et al.[19] and Chen et al.[20] used this model to predict the breakthrough curves in the expanded bed adsorption. When capturing proteins in an expanded bed with a high flow velocity, the slow diffusion rate of proteins results in high intraparticle diffusion resistance, significantly affecting the breakthrough curve. It is argued that, in this case, the particle size, characterizing the diffusion path in the adsorbent particles, should have a substantial effect on the breakthrough curves.[13] Therefore, simulation results should be improved when the particle size axial distribution and bed voidage axial variations are taken into account in the model. Tong et al.[17] modified the mathematical model by taking into account the particle size axial distribution in expanded beds. Following their experimental research using in-bed monitoring in expanded beds, Bruce et al.[12] predicted the in-bed breakthrough curves in expanded beds by using zonally measured parameters. Li et al.[21] developed a three-zone model to predict in-bed breakthrough curves and confirmed the effect of the particle size axial distribution and bed voidage axial variations on the breakthrough curves in expanded beds. Recently, Kaczmaarski et al.[22] also analyzed the effects of the axial and local particle size distribution and bed voidage axial variation on the breakthrough curves in expanded beds.

Up to now, theoretical and experimental researches have focused on protein adsorption onto Streamline DEAE or Streamline SP in expanded beds. Streamline DEAE and Streamline SP are first-generation adsorbents; the adsorbent matrix has low density and large particle diameter with wide particle size distribution (100–300 μm). The matrix of the second-generation adsorbent, Streamline direct CST I, has high density and small particle diameter with narrow particle size distribution (80–165 μm). In this study, BSA breakthrough curves in expanded bed adsorption are measured for both Streamline direct CST I and Streamline DEAE, and a mathematical model is developed to predict the breakthrough curves and to compare with the experimental results. The effects of intraparticle diffusion resistance, film mass transfer resistance, liquid axial dispersion, solid axial dispersions, adsorbent particle size axial distribution, and bed voidage axial variation on the breakthrough curves will be evaluated for expanded beds packed with Streamline DEAE and with Streamline direct CST I, respectively.

Although the adsorbents and the columns are designed specifically for expanded beds to maintain stable bed expansion, the liquid axial dispersion is more significant than that in fixed beds. Sometimes, some inadequate operation—such as the column not being in a vertical position, trapped air in the bottom distribution system, clogging of the bottom distribution system and pump pulse—would make the liquid axial dispersion more significant. Therefore, it is necessary to exactly measure and predict the liquid axial dispersion in expanded beds to allow stable bed expansion during protein adsorption.

Usually, the liquid axial dispersion coefficient in expanded beds is measured from residence time distribution (RTD) by using the moment method.[11,23-25] Based on the experimental data of RTD curves, the mean residence time and the variance of distribution can be calculated. Then, by letting the first absolute moment of the dispersion model equal the mean residence time, and the second central moment of the dispersion model equal the variance of distribution, the liquid axial dispersion coefficient can be obtained easily. However, the validity of the dispersion model cannot be judged by this moment analytical method because the fitting degree of the calculated response curves to that measured experimentally cannot be evaluated directly. Sometimes, it will cause a significant deviation for the estimation of the liquid axial dispersion coefficient with the baseline drift and baseline fluctuation of experimental RTD curves during measurements. Fernandez-Lahore et al.[26] fitted the experimental RTD curves with the theoretical model in Laplace domain using the expression originally developed by Villermaux et al.[27] In this paper, an analytical solution for diract input mode, in which liquid axial dispersion, tracer intraparticle diffusion, and film mass transfer all are taken into account, is used to fit experimental RTD curves to better estimate the liquid axial dispersion coefficient.

Experimental

Equipment

A pilot-scale Streamline 50 column (Amersham Pharmacia Biotech, Uppsala, Sweden) was used in all expanded bed experiments. Masterflex® peristaltic pumps (Cole-Parmer Instrument Co., Vernon Hills, IL) were used for buffer and feed application and to raise and lower the hydraulic adaptor of the

Streamline 50 column. A Jasco 7800 UV detector (Tokyo, Japan) equipped with a flowcell was used to monitor online BSA effluent concentration from the expanded bed and tracer (acetone) effluent concentration in RTD experiments, and the absorbance signal was logged using the data-acquisition software in a personal computer.

Adsorbents

Streamline DEAE and Streamline direct CST I were purchased from Amersham Pharmacia Biotech. Streamline DEAE is a weak anion exchanger with an $–O–CH_2CH_2–N^+(C_2H_5)_2H$ functional group, with the following characteristics: its matrix consists of macroporous crosslinked 6% agarose constraining crystalline quartz core materials, with a particle density of about 1200 kg/m^3, a particle size distribution of 100–300 μm, and a mean particle size of 200 μm. Streamline direct CST I is an ion exchanger with a multimodal functional group, with the following characteristics: its matrix consists of macroporous crosslinked 4% agarose constraining stainless steel core materials, with a particle density of about 1800 kg/m^3, a particle size distribution of 80–165 μm, and a mean particle size of 135 μm.

Model protein

The model protein, bovine serum albumin (BSA; product number A3059, further purified fraction V, ~99%), was purchased from Sigma (St. Louis, MO). The molecular weight of BSA is about 65,400 g mol^{-1}, diffusion coefficient at infinite dilution in water is about 6.15×10^{-11} m^2/s, radius of gyration is 29.8 Å, and isoelectric point is about 4.7.

A sample solution of BSA was prepared with the appropriate buffer; in the case of Streamline DEAE the buffer is 20 mM phosphate buffer (pH = 7.5), a mixture of Na_2HPO_4/NaH_2PO_4, and in the case of Streamline direct CST I the buffer is 50 mM acetate buffer (pH = 5), a mixture of acetate sodium and acetic acid. Distilled water was used in all experiments.

Batch adsorption experiments

Before performing adsorption isotherm experiments, the adsorbents must be saturated by phosphate buffer or acetate buffer. Adsorbents, in the amount of 0.5 mL by particle volume, are equilibrated with 30 mL of different concentrations of BSA solution about 8 h at 25°C on a shaking incubator (about 30 rpm); then BSA concentration in supernatant liquid is measured by UV 7800 detector at 280 nm (using a 2-mL quartz cuvette). The adsorption capacity is calculated by mass balance.

For the kinetic experiment 2 mL of adsorbent was mixed with 100 mL of BSA solution in a flask. The adsorption was carried out in the shaking incubator at 25°C at 150 rpm. Every few minutes, about 2 mL of the liquid phase was aspirated using a suction tube to determine protein concentration, and the sample was immediately returned to the vessel. By this procedure, the time course of BSA concentration in the batch adsorber was determined to estimate the effective pore diffusivity of BSA in Streamline DEAE and Streamline direct CST I.

Residence time distribution (RTD) experiments

A Streamline 50 column is packed either with 300 mL Streamline DEAE or with 300 mL Streamline direct CST I to maintain a stable expansion. For Streamline direct CST I, the settled bed height is 15.6 cm and the settled bed voidage is 0.39; for Streamline DEAE, the settled bed height is 16.5 cm and the settled bed voidage is 0.4. The liquid axial dispersion coefficient in expanded beds is measured by the RTD method. Acetone inert tracer is used in all RTD experiments. About 50% v/v concentration of acetone (1.5 mL buffer aqueous solution) is used for the dirac input mode, and input position at the bottom of the column.

Before carrying out the RTD measurement, the bed is expanded about 1 h by 20 mM phosphate buffer (pH = 7.5) for Streamline DEAE, and by 50 mM acetate buffer (pH = 5) for Streamline direct CST I. A dirac input of acetone sample is applied to the column at the bottom of the bed; the effluent liquid sample passes through the flowcell online, where the acetone concentration is monitored by UV detector at 280-nm wavelength; and the ABS (absorbance) signal of acetone is logged by the data-acquisition software in a personal computer.

Experimental procedures for the whole expanded bed adsorption process

Expansion/Equilibration Stage. First, the equilibration buffer is pumped through the column with upward flow to the expected expansion degree. Second, the expanded bed is allowed to stabilize at this degree of expansion for about 30–40 min. Then, the liquid axial dispersion in the expanded bed is checked by the RTD method; the liquid axial dispersion coefficient should be as small as possible by avoiding inadequate operation. The adaptor will be positioned about 0.5 cm above the height to which the bed expands, to reduce the dead volume in expanded beds.

Adsorption Stage. When the expanded bed is stable and equilibrated with the appropriate buffer, the process switches to feedstock application. Because of protein adsorption on adsorbents, the expanded bed height gradually drops, especially in the expanded bed of low-density Streamline DEAE; therefore, the liquid flow velocity will be increased gradually during the adsorption process to maintain a constant degree of bed expansion. The average liquid velocity was calculated from the ratio of total feed volume supplied to the column to the operation time in the loading process. The effluent stream from the top of the column will pass through the flowcell, where BSA effluent concentration is monitored online by UV 7800 detector, and the ABS (absorbance) signal of BSA is logged by the data-acquisition software in a personal computer. The BSA concentration in the feed was 2 kg/m^3, showing a linear relation between the UV detector signal (ABS) and BSA effluent concentration during the adsorption stage.

Washing Stage. When the measurement of the breakthrough curve was completed, the process switches to the wash buffer to wash out the excess protein, other loosely bound materials, and particulates from the column in the expanded mode until the effluent absorbance reaches a relative stable value. In the expanded bed of Streamline direct CST I, because of the highly favorable adsorption of BSA, the effluent absorbance approaches the baseline, meaning almost irreversible adsorption.

Elution Stage. After washing, the pump is turned off and the bed is allowed to settle. When the adsorbent has settled, the adaptor is moved down toward the surface until the edge of the

adaptor net touches the bed. Elution buffer is then pumped through the settled bed with a downward flow to elute BSA protein. Because the BSA concentration in the effluent is very high, the effluent samples are collected by small sample tubes, and the BSA concentration in these samples is then monitored by UV 7800 detector.

Mathematical Model for the Protein Adsorption in Expanded Beds

Mathematical model

The mathematical model is developed based on the work of Wright et al.,[14] where intraparticle diffusion, film mass transfer, liquid axial dispersion, and solid axial dispersion were taken into account. In addition, the particle size axial distribution and bed voidage axial variation in expanded beds are also included in the model.

The material balance equation for the liquid bulk phase in an expanded bed is

$$D_L \frac{\partial^2[\varepsilon_B(Z)C]}{\partial Z^2} - u\frac{\partial C}{\partial Z} - \varepsilon_B(Z)\frac{\partial C}{\partial t} - \frac{3k_f(Z)[1-\varepsilon_B(Z)]}{R(Z)} \times [C-(c)_{r=R(Z)}] = 0 \quad (1)$$

where D_L is the axial dispersion coefficient; C is the concentration in the fluid phase; u denotes superficial velocity; c is the concentration in the adsorbent pore; Z is the axial distance from column entrance; $\varepsilon_B(Z)$denotes bed voidage at the axial distance Z of the column, and thus $[1-\varepsilon_B(Z)]$ denotes the fractional volume taken up by the solid phase; r is the radial coordinate in the adsorbent particle; $R(Z)$ is the radius of the adsorbent at the axial distance Z of the column; t is the time; and $k_f(Z)$ is the film mass transfer coefficient at the axial distance Z of the column.

Boundary Conditions

$$D_L\left(\frac{\partial C}{\partial Z}\right)_{Z=0} = \frac{u}{\varepsilon_B(0)}[(C)_{Z=0}-C_0] \quad (1a)$$

$$\left(\frac{\partial C}{\partial Z}\right)_{Z=H} = 0 \quad (1b)$$

Initial Condition

$$t=0 \qquad C(Z,0)=0 \quad (1c)$$

The mass balance for adsorbent bulk phases in the expanded bed column is described as

$$[1-\varepsilon_B(Z)]\frac{\partial \bar{q}}{\partial t} = D_{ax,S}\frac{\partial^2 \bar{q}}{\partial Z^2} + [1-\varepsilon_B(Z)]\frac{3}{R(Z)}k_f(Z) \times [C-(c)_{r=R(Z)}] \quad (2)$$

where the $\bar{q}$ is the average adsorbent phase concentration and $D_{ax,S}$ is the solid axial dispersion coefficient in the expanded bed.

Boundary Conditions

$$\left(\frac{\partial \bar{q}}{\partial Z}\right)_{Z=0} = 0 \quad (2a)$$

$$\left(\frac{\partial \bar{q}}{\partial Z}\right)_{Z=H} = 0 \quad (2b)$$

Initial Condition

$$t=0 \qquad \bar{q}(Z,0)=0 \quad (2c)$$

The pore diffusion equation in the adsorbent is described as

$$\varepsilon_P\frac{\partial c}{\partial t} + \frac{\partial q}{\partial t} = D_e\left(\frac{\partial^2 c}{\partial r^2} + \frac{2}{r}\frac{\partial c}{\partial r}\right) \quad (3)$$

where q is the adsorbed amount concentration in adsorbent, ε_p is the particle porosity, and D_e is the adsorbate effective pore diffusivity.

Boundary Conditions

$$D_e\left(\frac{\partial c}{\partial r}\right)_{r=R(Z)} = \frac{R(Z)D_{ax,S}}{3[1-\varepsilon_B(Z)]}\frac{\partial^2 \bar{q}}{\partial Z^2} + k_f(Z)[C-(c)_{r=R(Z)}] \quad (3a)$$

$$\left(\frac{\partial c}{\partial r}\right)_{r=0} = 0 \quad (3b)$$

Initial Condition

$$t=0 \qquad c(r)=0 \qquad q(r)=0 \quad (3c)$$

In Eq. 3, the relationship between q and c depends on the adsorption equilibrium of the selected experimental system. Based on the experimental measurements for BSA protein adsorption on Streamline DEAE and on Streamline direct CST I, the Langmuir isotherm is assigned as

$$q = \frac{q_m c}{k_d + c} \quad (4)$$

where q_m is the adsorption capacity and k_d is the dissociation constant, both of which are determined by experiments.

The correlations recommended to estimate the particle size axial distribution and bed voidage axial variation in expanded beds, packed with the first-generation adsorbents, are

$$R(Z) = \frac{\bar{d}_p}{2}\left(1.20 - 0.51\frac{Z}{H}\right) \quad (5)$$

$$\varepsilon_B(Z) = \bar{\varepsilon}_B\left(0.629 + 0.738\frac{Z}{H}\right) \quad (6)$$

where the averaged adsorbent particle diameter $\bar{d}_p$ is an averaged value over the wider particle size distribution, and the bed averaged voidage $\bar{\varepsilon}_B$ is estimated as a function of the whole expanded bed height[28]

$$\bar{\varepsilon}_B = 1 - \left[(1 - \varepsilon_0) \frac{H_0}{H} \right] \tag{7}$$

where ε_0 and H_0 are the settled bed voidage and the settled bed height, respectively.

The correlations given by Eqs. 5 and 6 are based on the experimental data of Bruce et al.,[11] where a Streamline 50 column was packed with Streamline SP to measure both the particle size axial distribution and bed voidage axial variation in the expanded bed. Because that system is similar to our experimental setup, that is, a Streamline 50 column packed with Streamline DEAE (the same Streamline matrix), we used in the modeling the hydrodynamic results obtained by Bruce et al.[11] Kaczmarski et al.[22] recommended two different equations for the particle size axial distribution and bed voidage axial variation; simulated breakthrough curves using correlations from both groups[11,22] are similar.

Model parameters

The effective pore diffusivity D_e in adsorbents is determined by independent batch experiments.

The liquid axial dispersion coefficient D_L is measured experimentally during the expansion stage by the residence time distribution method.

The adsorbent axial dispersion coefficient $D_{ax,S}$ is estimated by the correlation of Van Der Meer et al.,[29] using experimental values for superficial velocity u, as follows

$$D_{ax,S} = 0.04u^{1.8} \text{ m}^2/\text{s} \tag{8}$$

The Wilson–Geankopolis equation,[30] applicable to low Reynolds number (Eq. 9), is used to estimate the film mass transfer coefficient $k_f(Z)$ in an expanded bed

$$\text{Sh} = \frac{1.09}{\varepsilon_B(Z)} \text{Re}^{1/3}\text{Sc}^{1/3} \qquad (0.0015 < \text{Re} < 55) \tag{9}$$

where Re is the Reynolds number $[=2R(Z)\rho u/\mu]$, Sc is the Schmidt number $[=\mu/(\rho D_m)]$, Sh is the Sherwood number $[=2k_f(Z)R(Z)/D_m]$, and D_m is the molecular diffusion coefficient.

Numerical method

The model equations are numerically solved by the orthogonal collocation method. Equations 1 and 2 are discretized at collocation points in the axial direction in the column, and Eq. 3 is discretized at collocation points in the particle radial direction, leading to a set of ordinary differential equations with initial values that are integrated in the time domain using Gear's stiff variable step integration routine. To obtain a stable numerical solution for a highly favorable adsorption isotherm, 21 bed axial collocation points and 21 particle radial collocation points are used.

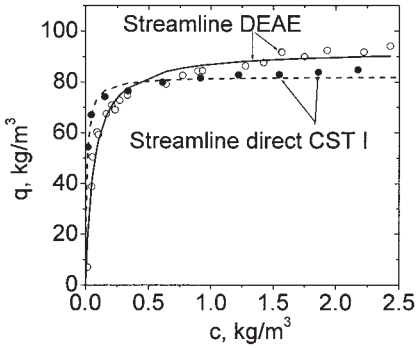

Figure 1. BSA adsorption isotherms on Streamline DEAE and on Streamline direct CST I at room temperature (~25°C).

Circle points: experimental data; lines: the calculated results by Langmuir equations, Eqs. 10a and 10b.

Results and Discussion

Adsorption isotherm and BSA effective pore diffusivity

Based on the independent batch adsorption equilibrium experiments, as shown in Figure 1, circle points represent the experimental data at room temperature (25°C). BSA protein adsorption isotherm on both Streamline DEAE and Streamline direct CST I can be approximately described by the Langmuir equation as follows.

BSA Adsorption on Streamline DEAE

$$q = \frac{92.59c}{0.065 + c} \tag{10a}$$

BSA Adsorption on Streamline Direct CST I

$$q = \frac{82.15c}{0.0109 + c} \tag{10b}$$

According to the Langmuir equation, the separation factor f can be defined as

$$f = \frac{1}{1 + c_0/k_d} \tag{11}$$

which characterizes the adsorption conditions. For a BSA concentration of 2 kg/m^3, which will be used in the adsorption kinetics experiments in batch adsorber and in expanded bed adsorption later, the separation factors are 0.032 for BSA adsorption on Streamline DEAE and 0.0055 for BSA adsorption on Streamline direct CST I, respectively, indicating highly favorable adsorption for BSA on Streamline adsorbents, especially on Streamline direct CST I (where virtually irreversible adsorption occurs).

Batch adsorption kinetic experiments are carried out to estimate BSA effective pore diffusivity in Streamline DEAE and in Streamline direct CST I; Figure 2 shows typical experimental data of the bulk concentration profiles in a batch adsorber (with 100 mL of 2 kg/m^3 BSA aqueous solution and 2 mL adsorbent).Then, the experimental data of the bulk concentra-

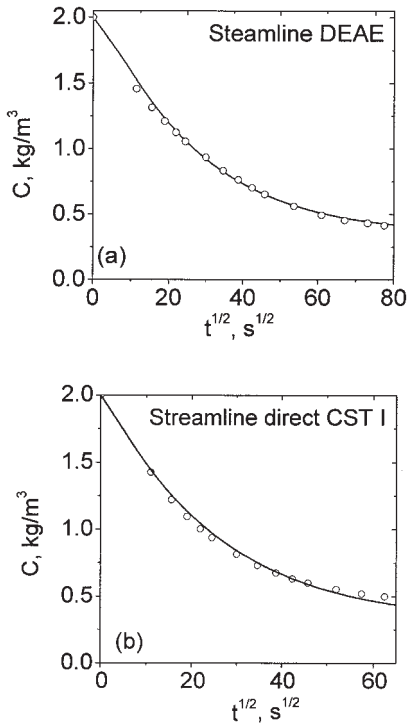

Figure 2. Estimation of BSA effective pore diffusivity in Streamline DEAE adsorbents and in Streamline CST I adsorbents in batch adsorber.

Circle points: experimental data; solid lines: simulation results of the pore diffusion model with $D_e = 3.2 \times 10^{-11}$ m^2/s and $k_f = 8.6 \times 10^{-6}$ m/s for Streamline DEAE (a) and with $D_e = 1.7 \times 10^{-11}$ m^2/s, and $k_f = \infty$ for Streamline direct CST I (b).

tion profile are fitted with the simulation results of the pore diffusion model to estimate BSA effective pore diffusion coefficient in Streamline DEAE as 3.2×10^{-11} m^2/s and in Streamline direct CST I as 1.7×10^{-11} m^2/s. It should be emphasized that in the pore diffusion model, the particle size is assigned an average particle diameter over the particle size distribution ($\bar{d}_p = 200$ μm for Streamline DEAE; $\bar{d}_p = 135$ μm for Streamline direct CST I), and the particle porosity is assigned a value of 0.55, according to the published literature.[31] The film mass transfer resistance is not negligible for BSA adsorption on Streamline DEAE; in contrast, the film mass transfer can be neglected for BSA absorption on Streamline direct CST I in the batch experimental system. A method to estimate both film mass transfer coefficient and effective pore diffusivity from a single bulk concentration–time curve in a batch adsorber has been reported elsewhere.[32]

Bed expansion and liquid axial dispersion coefficient in expanded bed

The expansion degree of expanded beds packed either with Streamline DEAE or with Streamline directs CST I is measured at various superficial flow velocities, as shown in Figure 3, where a Streamline 50 column is packed either with 300 mL Streamline DEAE or with 300 mL Streamline direct CST I; the settled bed height is 15.6 cm for Streamline direct CST I and 16.5 cm for Streamline DEAE. It is apparent that at the same degree of expansion, the superficial liquid flow velocity for the new Streamline direct CST I is higher than that for the old Streamline DEAE, given that the particle density of the "new" adsorbent (~1800 kg/m^3) is greater than that of the "old" adsorbent (~1200 kg/m^3). When the expansion degree is equal to 2, the superficial flow velocity for Streamline DEAE is only 228 cm/h, but for Streamline CST I, it allows a higher velocity of the feedstock (up to 553 cm/h) to pass through its expanded bed.

The residence time distribution method with a dirac tracer (acetone) input mode is used to estimate the liquid axial dispersion coefficient in expanded beds packed with Streamline DEAE and packed with Streamline direct CST I, respectively; the experimental data of RTD curves are shown in Figure 4, marked as circle points.

Based on the experimental data of RTD curves, the mean residence time ($\bar{t}_m$) and the variance of distribution (σ^2) are calculated as

$$\bar{t}_m = \frac{\int_0^\infty tCdt}{\int_0^\infty Cdt} = \frac{(\sum t_i C_i)\Delta t}{(\sum C_i)\Delta t} \tag{12}$$

$$\sigma^2 = \frac{\int_0^\infty t^2 Cdt}{\int_0^\infty Cdt} - \bar{t}_m^2 = \frac{(\sum t_i^2 C_i)\Delta t}{(\sum C_i)\Delta t} - \bar{t}_m^2 \tag{13}$$

If we then let the first absolute moment μ_1 of the dispersion model equal the mean residence time ($\bar{t}_m$) and the second central moment μ_2 of the dispersion model equal the variance of distribution (σ^2), the liquid axial dispersion coefficient can be easily obtained. Some common calculation formulas, Eq. 14,[33] Eq. 15,[11] and Eq. 16,[34] are summarized as follows:

$$\frac{\sigma^2}{\bar{t}_m^2} = \frac{2\bar{\varepsilon}_B D_L}{uH} \tag{14}$$

$$\frac{\sigma^2}{\bar{t}_m^2} = \frac{2(\bar{\varepsilon}_B D_L/uH) + 3(\bar{\varepsilon}_B D_L/uH)^2}{1 + 2(\bar{\varepsilon}_B D_L/uH) + (\bar{\varepsilon}_B D_L/uH)^2} \tag{15}$$

$$\frac{\sigma^2}{\bar{t}_m^2} = 2\frac{\bar{\varepsilon}_B D_L}{uH} - 2\left(\frac{\bar{\varepsilon}_B D_L}{uH}\right)^2 (1 - e^{-uH/(\bar{\varepsilon}_B D_L)}) \tag{16}$$

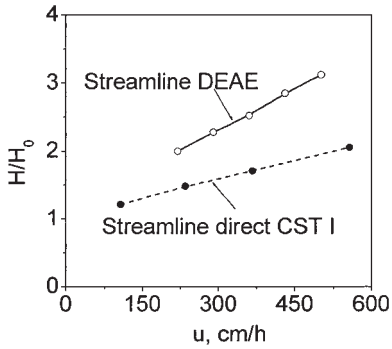

Figure 3. Relationship between bed expansion degree and superficial liquid flow velocity in expanded beds packed with Streamline DEAE and with Streamline CST I.

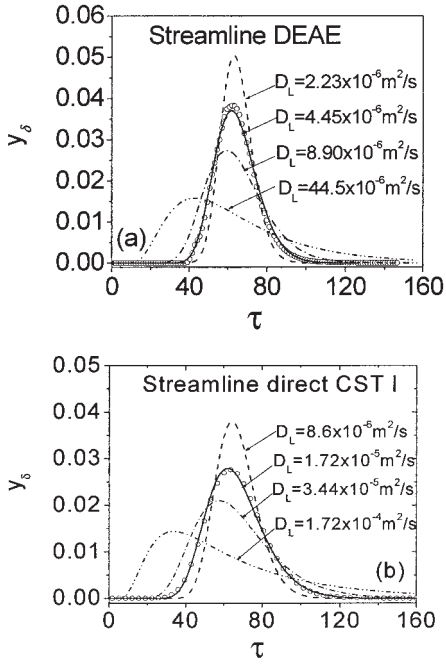

Figure 4. Experimental data of RTD curves are fitted by the analytical solution with the dirac input of acetone tracer at expanded beds packed with Streamline DEAE and packed with Streamline direct CST I.

(a) Settled bed height 16.5 cm, expanded degree as 2, superficial liquid flow velocity 228 cm/h, $\tau = D_p t/\bar{R}^2 = 0.128t$; (b) settled bed height as 15.6 cm, expansion degree as 2, superficial liquid flow velocity 553 cm/h, $\tau = D_p t/\bar{R}^2 = 0.281t$.

When considering the tracer intraparticle diffusion resistance, film mass-transfer resistance, and liquid axial dispersion, one has

$$\frac{\sigma^2}{\bar{t}_m^2} = \frac{2u\bar{R}^2\varepsilon_P^2}{15H}\frac{(1-\bar{\varepsilon}_B)}{[\bar{\varepsilon}_B+\varepsilon_p(1-\bar{\varepsilon}_B)]^2}\left(\frac{1}{\varepsilon_P D_P}+\frac{5}{k_f\bar{R}}\right)+\frac{2\bar{\varepsilon}_B D_L}{uH} \tag{17}$$

In Eq. 17, estimations of acetone intraparticle diffusivity and particle porosity for acetone are described in the Appendix.

The results calculated by different formulas are similar. Because of the small size of the tracer molecule, acetone, the effect of the tracer intraparticle diffusion is negligible. For Streamline DEAE, when the bed expands to about twice the settled bed height with 228 cm/h superficial flow velocity, the liquid axial dispersion coefficient is 4.45×10^{-6} m/s; for Streamline direct CST I, when the bed expands to about twice the settled bed height with 553 cm/h superficial flow velocity, the liquid axial dispersion coefficient increases to 17.2×10^{-6} m/s as a result of the liquid flow velocity increase. In the calculation, the mean residence time and variance of the residence time distribution of the sampling system and the precolumn tubing were subtracted from the measured mean residence time and variance of the overall residence time distribution to yield the corrected mean residence time and variance of the RTD of the expanded bed column. As an example, the mean residence time of extra-column volume and variance are $\bar{t}_c = 38$ s and $\sigma_c^2 = 352$ s^2 at 228 cm/h flow rate and $\bar{t}_c = 18$ s and $\sigma_c^2 = 126$ s^2 for 553 cm/h, respectively.

If there is a baseline drift or a baseline fluctuation for experimental RTD curves, the liquid axial dispersion coefficient estimated by the previous calculation method may deviate from the real value of liquid axial dispersion coefficients. Therefore, in Figure 4, the experimental data of RTD curves are fitted by the analytical solutions with the dirac input of acetone tracer to confirm the calculation accuracy, and at the same time, the parametric sensitivity is analyzed. The analytical solution is given in the Appendix for reference, in which the tracer intraparticle diffusion resistance, film mass transfer resistance, and liquid axial dispersion coefficient are all taken into account. In Figure 4, the mean residence time has been corrected, and the variance associated with extra-column volumes was negligible compared to the variance associated with the expanded bed.

BSA protein breakthrough behavior in expanded beds packed with Streamline direct CST I and with Streamline DEAE

BSA Breakthrough Behavior in Expanded Beds Packed with Streamline Direct CST I. When a given volume (300 mL) of Streamline direct CST I is packed into a Streamline 50 column, the settled bed height is 15.6 cm. BSA aqueous solution with concentration 2 kg/m^3 prepared with 50 mM acetate buffer (pH = 5) is introduced to the column in upward flow with 181 mL/min flow velocity. The experimental data of the BSA breakthrough curve are shown in Figure 5, marked as circle points.

The uniform model, where the model parameters are average values all over the column (average particle diameter and average bed voidage), is used to predict the breakthrough curve, as shown in Figure 5 (solid line). Because of the heavier adsorbent, Streamline direct CST I, with narrower particle size distribution (80–165 μm), the effects of the particle size axial distribution and the bed voidage axial variation on the breakthrough curves are smaller, so the uniform model predicts the breakthrough curve in expanded beds reasonably well.

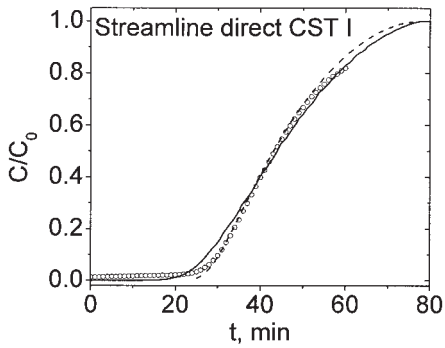

Figure 5. BSA breakthrough curve in expanded bed packed with Streamline direct CST I.

Circle points: experimental data; solid line: uniform model; dashed line: the analytical solution (Eq. 18) with irreversible adsorption ($q_m = 82.15$ kg/m^3). The experimental conditions and model parameters are summarized in Table 1.

Table 1. Experimental Conditions and Model Parameters Used for the Simulation of the Breakthrough Curves in Expanded Beds

Expanded Bed of Streamline Direct CST I	Expanded Bed of Streamline DEAE
$H_0 = 15.6$ cm	$H_0 = 16.5$ cm
$\bar{\varepsilon}_{B0} = 0.39$	$\bar{\varepsilon}_{B0} = 0.4$
$\bar{d}_p = 135\ \mu$m	$\bar{d}_p = 200\ \mu$m
$\varepsilon_p = 0.55$	$\varepsilon_p = 0.55$
$C_0 = 2$ kg/m^3	$C_0 = 2$ kg/m^3
$u = 15.37 \times 10^{-4}$ m/s*	$u = 7.10 \times 10^{-4}$ m/s*
$H = 32.0$ cm	$H = 33.5$ cm
$H/H_0 = 2.05$	$H/H_0 = 2.03$
$\bar{\varepsilon}_B = 0.7025$	$\bar{\varepsilon}_B = 0.7045$
$q_m = 82.15$ kg/m^3	$q_m = 92.59$ kg/m^3
$k_d = 0.0109$ kg/m^3	$k_d = 0.065$ kg/m^3
$D_e = 1.7 \times 10^{-11}$ m^2/s	$D_e = 3.2 \times 10^{-11}$ m^2/s
$D_L = 17.2 \times 10^{-6}$ m^2/s	$D_L = 4.45 \times 10^{-6}$ m^2/s
$k_f = 10.6 \times 10^{-6}$ m/s	$k_f = 6.6 \times 10^{-6}$ m/s
$D_{ax,S} = 3.45 \times 10^{-7}$ m^2/s	$D_{ax,S} = 8.78 \times 10^{-8}$ m^2/s

*u is the average value during the adsorption stage, with the interval minimum–maximum liquid velocity of 6.68–7.52 $\times 10^{-4}$ m/s for Streamline DEAE, and of 15.20–15.54 $\times 10^{-4}$ m/s for Streamline direct CST I.

The model parameters D_e, k_f, D_L, and $D_{ax,S}$ characterize the effects of intraparticle diffusion resistance, film mass-transfer resistance, liquid axial dispersion, and solid axial dispersion on the breakthrough curves during expanded bed adsorption. Figure 6 demonstrates the individual contribution of each model parameter (D_e, k_f, D_L, or $D_{ax,S}$) on the breakthrough curve during expanded bed adsorption. First, by controlling film mass transfer resistance, the liquid and solid axial dispersion must be as small as possible to neglect their effects on the breakthrough curves (k_f increased 10 times, D_L and $D_{ax,S}$ decreased 10 times); the effect of the model parameter D_e on the breakthrough curve is demonstrated in Figure 6, represented by a dashed line. It is apparent that the contribution of BSA effective pore diffusivity to the breakthrough curves is dominant (dashed line). Then, in turn, the effects of film mass transfer resistance, liquid axial dispersion, and solid axial dispersion are considered in the model; the simulation results are demonstrated in Figure 6, respectively. The dashed–double-dotted line represents the simulation result when both the intraparticle diffusion resistance and the film mass transfer resistance are taken into account in the model. By comparing with the simulation result (dashed line, considering only D_e), the effect of the film mass transfer coefficient is not negligible for such the highly favorable protein adsorption isotherm because the breakthrough time is significantly shortened as the result of the effect of k_f. The dashed-dotted line represents the simulation results where intraparticle diffusion resistance, film mass transfer resistance, and liquid axial dispersion are taken into account in the model, and the solid line represents the simulation results when intraparticle diffusion resistance, film mass transfer resistance, liquid axial dispersion, and solid axial dispersion all are taken into account in the model. It is apparent that the effects of the liquid axial dispersion coefficient and the solid axial dispersion coefficient are smaller even at high liquid flow velocity (up to 553 cm/h) if the bed expansion is stable.

Based on the simulation results, as shown in Figure 6, the effects of the liquid axial dispersion and solid axial dispersion on the breakthrough curves are smaller in a stable expanded bed packed with Streamline direct CST I. BSA protein adsorption on Streamline direct CST I is highly favorable, leading to almost irreversible adsorption (Figure 1); therefore, instead of the numerical solution, a simple analytical solution derived at the irreversible adsorption isotherm with $q_m = 82.15$ kg/m^3 (Eq. 18), which takes into account both the intraparticle diffusion and film mass transfer, may be used approximately to predict the breakthrough curves in the expanded bed (as shown in Figure 5, dashed line). The analytical solution is indeed close to the experimental data in expanded bed adsorption. Moreover, the analytical solution (dashed line in Figure 5) is similar to the simulated breakthrough curve from a model where only the intraparticle diffusion and film mass transfer are significant (dashed–double-dotted line in Figure 6). This analytical solution was reported by Weber and Chakravorti[35] based on the assumption of constant pattern, as follows

$$(\tau_1 - 1)N_{pore} = \frac{15}{\sqrt{3}}\tan^{-1}\left[\frac{2\eta+1}{\sqrt{3}}\right] - \frac{15}{2}\left[\ln(1+\eta+\eta^2) - \frac{1}{3}\right] + \frac{5}{\mathrm{Bi}}\left[\ln(1-\eta^3)+1\right] - \frac{5\pi}{2\sqrt{3}} \quad (18)$$

where the dimensionless parameters are defined as

$$\tau_1 = \frac{\left(\frac{ut}{H} - \bar{\varepsilon}_B\right)}{\Lambda} \qquad N_{pore} = \frac{15(1-\bar{\varepsilon}_B)D_e H}{u\bar{R}^2} \qquad \eta = \left(1 - \frac{C}{C_0}\right)^{1/3}$$

$$\Lambda = \frac{(1-\bar{\varepsilon}_B)q_m}{C_0} \qquad \mathrm{Bi} = \frac{k_f \bar{R}}{D_e}$$

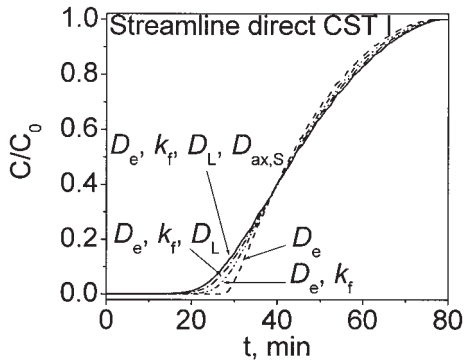

Figure 6. Contribution of each model parameter (D_e, k_f, D_L, or $D_{ax,[infi]S}$) to the breakthrough curve in expanded bed packed with Streamline direct CST I.

Dashed line: uniform model with $D_e = 1.7 \times 10^{-11}$ m^2/s (neglect k_f, D_L, and $D_{ax,S}$ effects); dashed–double-dotted line: uniform model with $D_e = 1.7 \times 10^{-11}$ m^2/s and $k_f = 10.6 \times 10^{-6}$ m/s (neglect D_L and $D_{ax,S}$ effects); dashed–dotted line: uniform model with $D_e = 1.7 \times 10^{-11}$ m^2/s, $k_f = 10.6 \times 10^{-6}$ m/s, and $D_L = 17.2 \times 10^{-6}$ m^2/s (neglect $D_{ax,S}$ effect); solid line: uniform model with considering D_e, k_f, D_L, and $D_{ax,S}$ effects ($D_e = 1.7 \times 10^{-11}$ m^2/s, $k_f = 10.6 \times 10^{-6}$ m/s, $D_L = 17.2 \times 10^{-6}$ m^2/s, and $D_{ax,S} = 3.45 \times 10^{-7}$ m^2/s). The other calculation conditions are the same as in Figure 5.

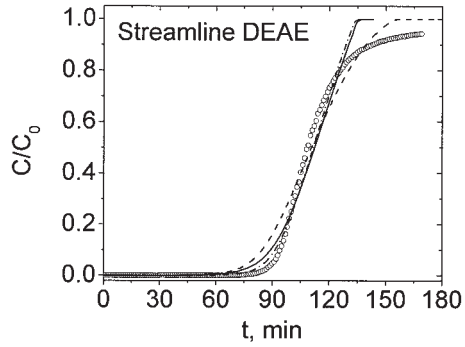

Figure 7. BSA breakthrough curve in expanded bed packed with Streamline DEAE.

Circle points: experimental data; dashed line: uniform model; solid line: modified uniform model; dashed–dotted line: modified uniform model with double k_f value. The experimental conditions and model parameters are summarized in Table 1.

It should be emphasized that this formula requires that $\tau_1 N_{pore} > 2.5 + 1/\mathrm{Bi}$.

The effects of particle size axial distribution, bed voidage axial variation, liquid axial dispersion, and solid axial dispersion on the breakthrough curve are smaller than those of intraparticle diffusivity and film mass-transfer coefficient for BSA adsorption in the expanded bed packed with streamline direct CST I; therefore, the uniform model and the analytical solution give a reasonable fit of experimental breakthrough curves. However, in the uniform model, the effects of the particle size axial distribution and bed voidage axial variation on the breakthrough curve are neglected, which results in predicted breakthrough curves slightly broader than the experimental data (greater amount of larger-size adsorbent at the bottom of the column and low amount of smaller-size adsorbent at the top of the column, will make the real breakthrough curve steeper). In the analytical solution, the effects of the particle size axial distribution and the bed voidage axial variation on the breakthrough curve (making the breakthrough curves slightly steeper), and the effects of the liquid axial dispersion and the solid axial dispersion on the breakthrough curve (making the breakthrough curves slightly broader) are all neglected; it happens that the sharpening effect almost equals the broadening effect for our experimental conditions, leading to an analytical solution that is closer to experimental data.

BSA Breakthrough Behavior in Expanded Beds Packed with Streamline DEAE. When Streamline DEAE (300 mL) is packed into a Streamline 50 column, the settled bed height is 16.5 cm. A 2 kg/m^3 BSA aqueous solution, prepared with 20 mM phosphate buffer (pH = 7.5) is introduced in upward flow at the column bottom with 83.6 mL/min flow velocity. The bed is expanded to about twice the settled bed height. The experimental data of the BSA breakthrough curve are shown in Figure 7, marked as circle points. First, the uniform model is used to predict the breakthrough curve, and the simulation result (dashed line, in Figure 7) is compared with the experimental data. The simulation result does not fit the experimental data very well.

Based on the experimental results, at the initial breakthrough stage, the real adsorption behavior in expanded beds is better than the predicted results by the uniform model; however, there is a tailing behavior of the breakthrough curves when the effluent concentration approaches the feed concentration. In previously published articles, the tailing behavior was explained by the presence of the dimer in BSA samples, or microporous diffusion in the macroporous adsorbent, or protein steric hindrance on active sites of the surface of the adsorbent. Until now, the explanation is still unclear for the tailing behavior of the breakthrough curves that often occur for both medium and large size protein adsorption. Because the Streamline adsorbents are macroporous, at the initial adsorption stage, the macroporous diffusion should be considered; that is, the breakthrough curves may be predicted by the macroporous diffusion model for the initial breakthrough stage.

For the protein adsorption in a stable expanded bed, the slow diffusion rate of macromolecular protein in adsorbent significantly affects the breakthrough behavior in the expanded bed. Therefore, the particle size should have an effect on the breakthrough curves as the result of particle diameter, characterizing the diffusion path in the adsorbent particle (small particle diameters having a shorter diffusion path length, leading to lower diffusion resistance than that in larger particle). Compared with Streamline direct CST I, Streamline DEAE has a wider particle size distribution (100–300 μm); when the bed expands, the smaller and lighter particles move to positions at the top of the expanded bed, the larger and heavier particles to the bottom, and more adsorbents will be present at the bottom of the column. At the top zone of the column there is a small amount of adsorbent, and thus the real adsorption behavior in expanded beds is better than the predicted result by the uniform mode. The simulation result by the modified uniform model with taking into account the particle size axial distribution (Eq. 5) and bed voidage axial variation (Eq. 6) is shown in Figure 7, denoted by the solid line. Compared with the uniform model, the simulation results with the modified uniform model better describe the initial breakthrough. For such a highly favorable adsorption isotherm, BSA protein diffuses by a shrinking core mode in the Streamline DEAE, so the more significant effect of the particle size axial distribution and bed voidage axial variation on the breakthrough curves will be observed at the end of the breakthrough curves, and not at the initial breakthrough stage. In our previous work[21] for the small-size protein (lysozyme) adsorption on Streamline SP in expanded beds, where the tailing behavior of the breakthrough curves was not observed, a significant improvement in the simulation results by the modified uniform model can be observed.

In Figure 8, we give the detailed comparisons among three simulation results: the dashed line represents the uniform model, the dashed-dotted line represents the modified uniform model by taking into account the particle size distribution, and the solid lines represent the modified uniform model by taking into account both the particle size distribution and bed voidage axial variation. From Figure 8, by comparing the simulation results of the uniform model (dashed line) and modified uniform model with particle size axial distribution (dashed–dotted line), the effect of the particle size distribution on the breakthrough curve is significant; however, by comparing the simulation results of the modified uniform model with particle size axial distribution (dashed–dotted line) and the modified uniform model with both particle size axial distribution and bed voidage axial variation (solid line), the effect of the bed voidage axial variation on the breakthrough curve is small. It should

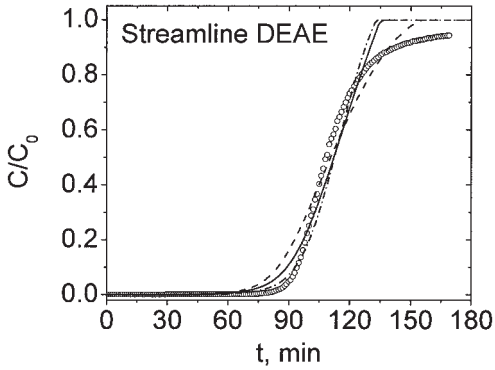

Figure 8. Effect of the particle size axial distribution and bed voidage axial distribution on the breakthrough curves in expanded beds.

Circle points: experimental data; dashed line: uniform model; dash–dotted line: modified uniform model with considering particle size axial distribution; solid line: modified uniform model with considering both particle size axial distribution and bed voidage axial distribution. The experimental conditions and model parameters are the same as in Figure 7.

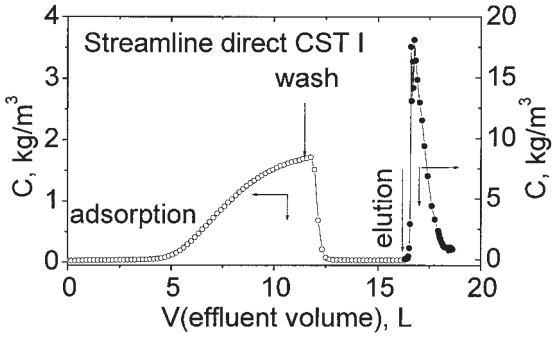

Figure 9. Effluent curves of BSA protein during adsorption, washing, and elution stages in expanded bed packed with Streamline direct CST I.

At the adsorption stage, 2 kg/m^3 BSA aqueous solution, prepared with 50 mM acetate buffer, pH = 5, is applied from the bottom of the expanded bed at 181 mL/min flow velocity; at the washing stage, 50 mM acetate buffer, pH = 5, is applied from the bottom of the expanded bed; and at the elution stage, 50 mM acetate buffer with 1 M NaCl, pH = 7, is applied from the top of the settled bed at 39 mL/min flow rate.

be emphasized that there is an effect of bed voidage axial variation on the breakthrough curve when adsorbents have larger particle diameter with wider particle size distribution. Kaczmarski and Bellot[22] claimed that the bed voidage axial variation had no effect on breakthrough curves only for the case of smaller-size adsorbents ($\bar{d}_p$ values of 50 or 150 μm) with relatively narrow particle size distribution.

It is observed that the real bed adsorption behavior at the initial breakthrough stage is still better than the predicted results even if we modify the uniform model by taking into account the particle size axial dispersion and bed voidage axial variation. Based on the theoretical analysis, as shown in Figure 6, the film mass transfer coefficient also has an important effect on the breakthrough time for such a highly favorable adsorption isotherm. It is very important to correctly estimate k_f in the simulation. From the published the papers, the film mass transfer coefficient k_f is estimated by the correlations for fixed beds or their revised formula. In expanded beds, the adsorbent particles are suspended in the liquid phase and fluctuate slightly up and down, which will favor the film mass transfer; that is, the real k_f value should be larger than the estimated value of k_f by the previous correlations. In Figure 7, simulation results with double k_f value ($k_f \cong 13.2 \times 10^{-6}$ m/s) will more nearly reflect the real breakthrough time.

Comprehensive evaluations on the whole expanded-bed protein adsorption process with Streamline DEAE and with Streamline CST I

Experiments are carried out for the whole expanded-bed BSA protein adsorption process with Streamline direct CST I (Figure 9) and with Streamline DEAE (Figure 10). A Streamline 50 column is packed either with Streamline direct CST I or Streamline DEAE at the same amount of the adsorbents (300 mL). With the same degree of expansion (twice the settled bed height), 2 kg/m^3 BSA aqueous solution is applied to the expanded beds and BSA protein is adsorbed by the adsorbents; after the adsorption stage, the bed is washed and BSA protein recovery proceeds at the elution stage. The detailed operation procedures have been previously described.

Based on the experimental results shown in Figures 9 and 10, the comprehensive evaluations on the hydrodynamics, BSA dynamic adsorption capacity, and BSA recovery in the expanded bed adsorption process with Streamline DEAE and with Streamline direct CST I are summarized as follows:

(1) For the same degree of expansion and the same expanded bed height, the high-density Streamline direct CST I allows a higher feed flow velocity (553 cm/h) to pass through the expanded bed; in contrast, a low feed flow velocity (259 cm/h) is allowed to pass through the expanded bed packed with low-density Streamline DEAE. Because of the high flow velocity, the liquid axial dispersion coefficient is correspondingly increased in expanded beds of Streamline direct CST I. Based on our experimental and theoretical research on the BSA break-

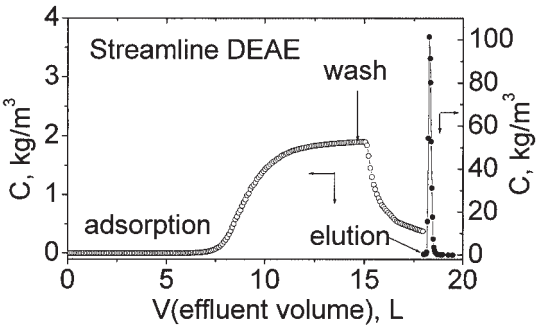

Figure 10. Effluent curves of BSA protein during adsorption, washing, and elution stages in expanded bed packed with Streamline DEAE.

At the adsorption stage, 2 kg/m^3 BSA aqueous solution, prepared with 20 mM phosphate buffer, pH = 7.5, is applied from the bottom of the expanded bed at 83.6 mL/min flow velocity; at the washing stage, 20 mM phosphate buffer, pH = 7.5, is applied from the bottom of the expanded bed; and at the elution stage, 20 mM phosphate buffer with 0.5 M NaCl, pH = 7.5, is applied from the top of the settled bed at 37 mL/min flow rate.

through behavior in an expanded bed of Streamline direct CST I, the effect of the liquid axial dispersion on the breakthrough curve is also slight, even at such a high flow velocity if the bed expansion is stable.

(2) At 5% BSA breakthrough point during expanded bed adsorption, BSA dynamic binding capacity on Streamline direct CST I is 34 mg (BSA)/mL of settled bed volume and BSA dynamic binding capacity on Streamline DEAE is 50 mg (BSA)/mL of settled bed volume. However, BSA binding capacity on Streamline direct CST I is not sensitive to ionic strength in feedstock, which means there is no need for dilution of feedstock arising from high ionic strength. In contrast, BSA binding capacity on Streamline DEAE is very sensitive to the ionic strength in feedstock; when the ionic strength in feedstock is increased to 50 mM, the BSA adsorption capacity decreases by half. BSA dynamic binding capacity, $Q_{5\%}$, is calculated from the BSA breakthrough curve at expanded bed adsorption stage; the formula is defined as

$$Q_{5\%} = \frac{\int_0^{V_{5\%}} (C_0 - C)dV}{V_A} \tag{19}$$

where V is the effluent liquid volume from expanded beds, $V_{5\%}$ is the effluent liquid volume at 5% BSA breakthrough point, and V_A is the settled bed volume of adsorbents.

(3) At the washing stage, it is found that BSA effluent concentration quickly decreases and approaches the baseline for the expanded bed of Streamline direct CST I, which means almost irreversible adsorption for BSA binding to Streamline CST I. BSA adsorption on Streamline DEAE is reversible; when washing, some BSA can be desorbed from Streamline DEAE so that the effluent concentration approaches a relatively stable value.

(4) The ligand of Streamline DEAE is very sensitive to salt concentration in buffer, so BSA adsorbed on Streamline DEAE can be eluted easily by increasing the salt concentration to 0.5 M in 20 mM phosphate buffer, pH = 7.5. BSA recovery in the whole expanded bed adsorption process can reach 91%. From the BSA effluent concentration curve during the elution stage, it is observed that BSA can be eluted almost completely from Streamline DEAE; however, as a result of desorption during the washing stage, BSA recovery is not up to 100%—a small amount of the elution buffer is consumed, as shown in Figure 10. Streamline direct CST I has a multimodal ligand that is not sensitive to the salt concentration. Therefore, it is very difficult to elute BSA from Streamline CST I in the column only by increasing the salt concentration in 50 mM acetate buffer, pH = 5. Therefore, to accomplish elution of adsorbed BSA proteins, both salt concentration and pH value in acetate buffer are increased. Here, when the elution buffer is 50 mM acetate buffer with 1 M NaCl at pH = 7, BSA recovery is up to 87%. From the BSA effluent concentration curve during the elution stage, it can be noted that BSA cannot be eluted completely, and the amount of the elution buffer consumed is also greater, as shown in Figure 9.

Conclusions

With the specially designed adsorbents (Streamline DEAE and Streamline direct CST I), a stable expanded bed can be formed. At the same degree of expansion, the high-density Streamline direct CST I allows a higher feed flow velocity to pass through the expanded bed; in contrast, a lower feed flow velocity is allowed to pass through the expanded bed of lower-density Streamline DEAE. With the high feed flow velocity, the liquid axial dispersion is more significant in the expanded bed of Streamline direct CST I than that in the expanded bed of Streamline DEAE.

In spite of the existence of intraparticle diffusion resistance, film mass transfer resistance, liquid axial dispersion, and solid axial dispersion during expanded bed adsorption, the contribution of BSA effective pore diffusivity to the breakthrough curves is dominant. The film mass transfer coefficient has a significant effect on the initial breakthrough time for the highly favorable protein adsorption isotherm; liquid axial dispersion and solid axial dispersion have a lesser effect on the breakthrough curves, even at high liquid flow velocity (up to 553 cm/h for Streamline direct CST I), if the bed expansion is stable.

Because of the narrow particle size distribution of Streamline direct CST I, the effects of the particle size axial dispersion and the bed voidage axial variation on the breakthrough behavior in the expanded bed are small, and thus the uniform model can be used to predict the breakthrough curves with acceptable accuracy. In contrast, because of the wide particle size distribution of Streamline DEAE, the effects of the particle size axial distribution and bed voidage axial variation on the breakthrough curves in the expanded bed should be taken into account in the model.

Based on the experimental results, at 5% BSA breakthrough point during expanded bed adsorption, the BSA dynamic binding capacity on Streamline DEAE is 50 mg (BSA)/mL of settled bed volume, larger than that on Streamline direct CST I (34 mg (BSA)/mL of settled bed volume). However, the BSA binding capacity on Streamline CST I is not sensitive to ionic strength in the feedstock, which means there is no need for dilution of feedstock even at high ionic strength. In contrast, the BSA binding capacity on Streamline DEAE is very sensitive to the ionic strength in the feedstock; when the ionic strength in the feedstock is increased to 50 mM, BSA adsorption capacity decreases by half.

The ligand of Streamline DEAE is very sensitive to salt concentration in the buffer, so BSA adsorbed on Streamline DEAE can be easily eluted by increasing the salt concentration to 0.5 M in 20 mM phosphate buffer, pH = 7.5. BSA recovery in the whole expanded bed adsorption process reaches 91%, and a slight amount of the elution buffer is consumed. Streamline direct CST I has a multimodal ligand that is not sensitive to the salt concentration. Both salt concentration and pH value should be increased in the elution buffer; for example, 50 mM acetate buffer with 1 M NaCl, pH = 7, is used as the elution buffer in this experiment, and BSA recovery in the whole expanded bed adsorption process is up to 87%, and the amount of the elution buffer is greater than that consumed for Streamline DEAE. In addition, from the BSA effluent concentration curve during the elution stage, it is observed that BSA cannot be eluted completely from Streamline CST I.

Acknowledgments

We acknowledge financial support from Fundação para a Ciência e Tecnologia (FCT Grant SFRH/BD/6762/2001).

Notation

Bi = Biot number
c = concentration in particle pore, kg/m^3
C = concentration in fluid, kg/m^3
C_0 = inlet concentration in fluid, kg/m^3
$\bar{d}_p$ = average diameter of adsorbent, m
D_L = liquid axial dispersion coefficient, m^2/s
D_m = molecular diffusion coefficient, m^2/s
D_p = intraparticle pore diffusivity, m^2/s
D_e = intraparticle effective pore diffusivity, m^2/s
$D_{ax,S}$ = solid axial dispersion coefficient, m^2/s
H_0 = settled bed height, m
H = expanded bed height, m
k_d = dissociation constant defined by Eq. 4, m^3/kg
k_f = film mass transfer coefficient, m/s
n = amount of sample injected, kg
Pe = Peclet number
q = adsorbed concentration in adsorbent, kg/m^3 particle
$\bar{q}$ = averaged adsorbent phase concentration, kg/m^3
q_m = maximum adsorbed concentration, defined by Eq. 4, kg/m^3 particle
r = radial distance from center of particle, m
R = radius of adsorbent, m
Re = Reynolds number
Sc = Schmidt number
Sh = Sherwood number
t = time, s
u = superficial liquid flow velocity, m/s
V_c = column volume, m^3
Z = axial distance from column entrance, m

Greek letters

ε_0 = settled bed voidage, m^3/m^3
ε_B = bed voidage of expanded bed, m^3/m^3
ε_p = adsorbent porosity, m^3/m^3
μ = liquid viscosity, Pa·s
ρ = liquid density, kg/m^3

Literature Cited

1. Chase HA. Purification of proteins by adsorption chromatography in expanded beds. *Trends Biotechnol.* 1994;12:296-303.
2. Hjorth R. Expanded bed adsorption in industrial bioprocessing: Recent developments. *Trends Biotechnol.* 1997;15:230-235.
3. Thommes J, Bader A, Halfar M, Karau A, Kula MR. Isolation of monoclonal antibodies from cell containing hybridoma broth using a protein A coated adsorbent in expanded beds. *J Chromatogr.* 1996; 752:111-122.
4. Ujam LB, Clemmitt RH, Clarke SA, Brooks RA, Rushton N, Chase HA. Isolation of monocytes from human peripheral blood using immuno-affinity expanded-bed adsorption. *Biotechnol Bioeng.* 2003;83: 554-566.
5. Clemmitt RH, Chase HA. Direct recovery of glutathione S-transferase by expanded bed adsorption: Anion exchange as an alternative to metal affinity fusions. *Biotechnol Bioeng.* 2002;77:776-785.
6. Smith MP, Bulmer MA, Hjorth R, Titchener-Hooker NJ. Hydrophobic interaction ligand selection and scale-up of an expanded bed separation of an intracellular enzyme from Saccharomyces cerevisiae. *J Chromatogr A.* 2002;968:121-128.
7. Bai Y, Glatz CE. Capture of a recombinant protein from unclarified canola extract using Streamline expanded bed anion exchange. *Biotechnol Bioeng.* 2003;81:855-864.
8. Anspach FB, Curbelo D, Hartmann R, Garke G, Deckwer WD. Expanded-bed chromatography in primary protein purification. *J Chromatogr A.* 1999;865:129-144.
9. Jahanshahi M, Sun Y, Santos E, Pacek A, Franco TT, Nienow A, Lyddiatt A. Operational intensification by direct product sequestration from cell disruptates—Application of a pellicular adsorbent in a mechanically integrated disruption-fluidised bed adsorption process. *Biotechnol Bioeng.* 2002;80:201-212.
10. Chang YK, Chase HA. Development of operating conditions for protein purification using expanded bed techniques: The effect of the degree of bed expansion on adsorption performance. *Biotechnol Bioeng.* 1996;49:512–526.
11. Bruce LJ, Chase HA. Hydrodynamics and adsorption behaviour within an expanded bed adsorption column studied using in-bed sampling. *Chem Eng Sci.* 2001;56:3149-3162.
12. Bruce LJ, Chase HA. The combined use of in-bed monitoring and an adsorption model to anticipate breakthrough during expanded bed adsorption. *Chem Eng Sci.* 2002;57:3085-3093.
13. Karau A, Benken C, Thommes J, Kula MR. The influence of particle size distribution and operating conditions on the adsorption performance in fluidized beds. *Biotechnol Bioeng.* 1997;55:54-64.
14. Wright PR, Glasser BJ. Modeling mass transfer and hydrodynamics in fluidized-bed adsorption of proteins. *AIChE J.* 2001;47:474-488.
15. Willoughby N, Habib G, Hoare M, Hjorth R, Titchener-Hooker NJ. The use of rapid on-line monitoring of products and contaminants from within an expanded bed to control separations exhibiting fast breakthrough characteristics and to maximize productivity. *Biotechnol Bioeng.* 2000;70:254-261.
16. Willoughby NA, Hjorth R, Titchener-Hooker NJ. Experimental measurement of particle size distribution and voidage in an expanded bed adsorption system. *Biotechnol Bioeng.* 2000;69:648-653.
17. Tong XD, Xue B, Sun Y. Modeling of expanded-bed protein adsorption by taking into account the axial particle size distribution. *Biochem Eng J.* 2003;16:265-272.
18. Yun JX, Yao SJ, Lin DQ, Lu MH, Zhao WT. Modeling axial distributions of adsorbent particle size and local voidage in expanded bed. *Chem Eng Sci.* 2004;59:449-457.
19. Tong XD, Dong XY, Sun Y. Lysozyme adsorption and purification by expanded bed chromatography with a small-sized dense adsorbent. *Biochem Eng J.* 2002;12:117-124.
20. Chen WD, Dong XY, Sun Y. Modeling of the whole expanded-bed protein adsorption process with yeast cell suspensions as feedstock. *J Chromatogr A.* 2003;1012:1-10.
21. Li P, Xiu GH, Rodrigues AE. A 3-zone model for protein adsorption kinetics in expanded beds. *Chem Eng Sci.* 2004;59:3837-3847.
22. Kaczmarski K, Bellot JC. Theoretical investigation of axial and local particle size distribution on expanded bed adsorption process. *Biotechnol Process.* 2004;20:786-792.
23. Palsson E, Axelsson A, Larsson PO. Theories of chromatographic efficiency applied to expanded beds. *J Chromatogr A.* 2001;912:235-248.
24. Thommes J, Weiher M, Karau A, Kula MR. Hydrodynamics and performance in fluidized-bed adsorption. *Biotechnol Bioeng.* 1995;48: 367-374.
25. Fenneteau F, Aomari H, Chahal P, Legros R. Modeling of scale-down effects on the hydrodynamics of expanded bed adsorption columns. *Biotechnol Bioeng.* 2003;81:790-799.
26. Fernandez-Lahore HM, Kleef R, Kula MR, Thommes J. The influence of complex biological feedstock on the fluidization and bed stability in expanded bed adsorption. *Biotechnol Bioeng.* 1999;64:484-496.
27. Villermaux J, van Swaaij WPM. Modele representativ de la distribution des temps de sejour dans un reacteur semi-infini a dispersion axiale avec zones stagnantes. Application a l'ecoulement ruisselant dans des colonnes d'anneaux Raschig. *Chem Eng Sci.* 1969;24:1097-1111.
28. McCabe WL, Smith JC, Harriott P. *Unit Operations of Chemical Engineering*. 4th Edition. New York, NY: McGraw-Hill; 1985.
29. Van Der Meer AP, Blanchard CMRJP, Wesselingh JA. Mixing of particles in liquid fluidized beds. *Chem Eng Res Des.* 1984;62:214-222.
30. Wilson EJ, Geankopl CJ. Liquid mass transfer at very low Reynolds numbers in packed beds. *Ind Eng Chem Fundam.* 1966;5:9-14.
31. Boyer PM, Hsu JT. Experimental studies of restricted protein diffusion in an agarose matrix. *AIChE J.* 1992;38:259-272.
32. Li P, Xiu GH, Rodrigues AE. Modeling separation of proteins by inert core adsorbent in a batch adsorber. *Chem Eng Sci.* 2003;58:3361-3371.
33. Airs R. Notes on the diffusion-type model for longitudinal mixing in flow. *Chem Eng Sci.* 1959;9:266-267.

34. Levenspiel O. *Chemical Reaction Engineering*. 3rd Edition. New York, NY: Wiley; 1999.
35. Weber TW, Chakravorti RK. Pore and solid diffusion models for fixed-bed adsorbers. *AIChE J.* 1974;20:228-238.
36. Li P, Xiu GH, Rodrigues AE. Analytical breakthrough curves for inert core adsorbent with sorption kinetics. *AIChE J.* 2003;49:2974-2979.
37. Xiu GH, Nitta T, Li P, Jin G. Breakthrough curves for fixed-bed adsorbers: Quasi-lognormal distribution approximation. *AIChE J.* 1997;43:979-985.
38. Rasmuson A, Neretnieks I. Exact solution of a model for diffusion in particles and longitudinal dispersion in packed beds. *AIChE J.* 1980; 26:686-690.

Appendix: Analytical Solution for the Residence Time Distribution (RTD) Curve

In the mathematical model, the liquid axial dispersion, intraparticle diffusion, and film mass transfer resistance are all taken into account. The material balance equation for fluid phase is

$$D_L \frac{\partial^2 C}{\partial Z^2} - \frac{u}{\bar{\varepsilon}_B}\frac{\partial C}{\partial Z} - \frac{\partial C}{\partial t} - \frac{(1-\bar{\varepsilon}_B)}{\bar{\varepsilon}_B}\frac{3}{\bar{R}}\varepsilon_P D_p\left(\frac{\partial c}{\partial r}\right)_{r=\bar{R}} = 0 \tag{A1}$$

The material balance equation in pore particle is

$$\varepsilon_p \frac{\partial c}{\partial t} = \varepsilon_p D_p\left(\frac{\partial^2 c}{\partial r^2} + \frac{2}{r}\frac{\partial c}{\partial r}\right) \qquad (0 \le r \le \bar{R}) \tag{A2}$$

The initial and boundary conditions for Eqs. A1 and A2 are

$$C(Z, 0) = 0 \tag{A3}$$

$$c(r, Z, 0) = 0 \tag{A4}$$

$$C(0, t) = C^0 t_c \delta(t) \qquad \text{with dirac input mode} \tag{A5}$$

$$C(\infty, t) \qquad \text{is limited} \tag{A6}$$

$$\left(\frac{\partial c}{\partial r}\right)_{r=0} = 0 \tag{A7}$$

$$\varepsilon_P D_p\left(\frac{\partial c}{\partial r}\right)_{r=\bar{R}} = k_f[C - (c)_{r=\bar{R}}] \tag{A8}$$

Based on published works,[36-38] the analytical solution for the RTD curve at dirac input mode, is

$$y_\delta(\tau) = \frac{1}{\pi}\int_0^\infty \exp\left(\frac{\mathrm{Pe}\zeta}{2} - \zeta\sqrt{\frac{\sqrt{a^2+b^2}+a}{2}}\right)\times \cos\left(\beta\tau - \zeta\sqrt{\frac{\sqrt{a^2+b^2}-a}{2}}\right)d\beta \tag{A9}$$

where

$$a = \mathrm{Pe}\left[\frac{\mathrm{Pe}}{4} + 3\theta\upsilon\frac{\mathrm{Bi}^2 I_1 + \mathrm{Bi}(I_1^2 + I_2^2)}{(\mathrm{Bi}+I_1)^2 + I_2^2}\right] \tag{A10}$$

$$b = \theta\mathrm{Pe}\left[\beta + 3\upsilon\frac{\mathrm{Bi}^2 I_2}{(\mathrm{Bi}+I_1)^2 + I_2^2}\right] \tag{A11}$$

$$I_1 = \sqrt{\frac{\beta}{2}}\left(\frac{\sinh\sqrt{2\beta} + \sin\sqrt{2\beta}}{\cosh\sqrt{2\beta} - \cos\sqrt{2\beta}}\right) - 1 \tag{A12}$$

$$I_2 = \sqrt{\frac{\beta}{2}}\left(\frac{\sinh\sqrt{2\beta} - \sin\sqrt{2\beta}}{\cosh\sqrt{2\beta} - \cos\sqrt{2\beta}}\right) \tag{A13}$$

The dimensionless variables are

$$y(\delta) = \frac{C}{C^0\tau_c} \qquad \zeta = \frac{Z}{H} \qquad \upsilon = \left(\frac{1-\bar{\varepsilon}_B}{\bar{\varepsilon}_B}\right)\varepsilon_p \qquad \mathrm{Bi} = \frac{k_f\bar{R}}{\varepsilon_p D_p}$$

$$\theta = \frac{\bar{\varepsilon}_B H D_p}{u\bar{R}^2} \qquad \mathrm{Pe} = \frac{uH}{\bar{\varepsilon}_B D_L} \qquad \tau = \frac{D_p t}{\bar{R}^2}$$

where the reference concentration is the ratio between the amount injected and the fluid volume in the column, $C^0 = n/\bar{\varepsilon}_B V_c$ and $\tau_c = D_p t_c/\bar{R}^2$ ($t_c = \bar{\varepsilon}_B H/u$ is the space time).

The tracer (acetone) intraparticle pore diffusivity is estimated approximately as $D_p = 1.28 \times 10^{-9}$ m^2/s; the film mass transfer coefficient k_f is estimated by the correlation Eq. 9; and the particle porosity for acetone is estimated by first moment μ_1, equal to the mean resistance time of the experimental RTD curve, as suggested by Boyer and Hsu.[31]

Manuscript received Dec. 13, 2004, and revision received Feb. 22, 2005.